International Journal of Engineering

J o u r n a l   H o m e p a g e :   w w w . i j e . i r

Numerical Investigation of Magnetic Field Effects on Mixed Convection Flow in a Nanofluid-filled Lid-driven Cavity

J. Rahmannezhad[a], A. Ramezani[b], M. Kalteh* [c]

[a] *Department of Mechanical Engineering, University of Birjand, Birjand, Iran*
[b] *Faculty of Aerospace Engineering, K.N. Toosi University of Technology, Tehran, Iran*
[c] *Department of Mechanical Engineering, University of Guilan, Rasht, Iran*

PAPER INFO

ABSTRACT

In this work, the stencil adaptive method is applied to investigate the effects of a magnetic field on mixed convection of Al_2O_3-water nanofluid in a square lid-driven cavity. The incompressible Navier-Stokes equations are solved by an adaptive mesh method which has superior numerical advantages compared to the traditional method on the uniform fine grid. The main objective of this study is to investigate the influence of several pertinent parameters such as the Reynolds number, the Hartmann number and the solid particle volume fraction on the heat transfer performance of the nanofluid. Based on the obtained numerical results, the heat transfer rate increases with an increase of the Reynolds number but, it decreases with an increase of the Hartmann number. In addition, the results indicate that enhancement in heat transfer performance of the nanofluid with respect to that of the base fluid is depended on the Reynolds number.

NOMENCLATURE

B_0	magnetic field strength		X, Y	dimensional coordinates, m
Cp	specific heat, J/kg °K		**Greek Symbols**	
g	gravitational acceleration, m/s^2		α	thermal diffusivity
H	enclosure height, m		β	thermal expansion coefficient
Ha	Hartmann number		δ	solid particle volume fraction
k	thermal conductivity, W/m °K		μ	viscosity
Nu_{av}	average Nusselt number		ρ	density
Nu_{Y*}	local Nusselt number on the left hot wall		σ	electrical conductivity
Pr	Prandtl number		**Subscripts**	
Ra	Rayleigh number		f	fluid phase
Re	Reynolds number		max	maximum
T	dimensional temperature		nf	nanofluid
U, V	dimensional velocity components, m/s		s	solid phase
Up	lid velocity, m/s		**Superscript**	
W	enclosure width, m		*	nondimensional term

*Corresponding Author Email: mkalteh@guilan.ac.ir (M. Kalteh)

1. INTRODUCTION

Mixed convection heat transfer in cavities with moving walls is of great significance in many engineering applications like the cooling systems of electronic devices, solar collectors, crystal growth, lubrication technologies and food storage industry [1]. In a cavity, the movement of one of the walls creates a forced convection condition while buoyancy driven secondary flow is generated by the temperature difference across the walls. This flow regime is treated as mixed convection and it has complicated patterns of heat and mass transfer.

Low thermal conductivity of conventional fluids such as water and ethylene glycol imposes some limitations on the enhancement of heat transfer on the compactness of many engineering electronic devices. Nanofluids which are composed of nanometer-sized particles such as carbide ceramics, oxide ceramics, nitride ceramics, metals and semiconductors suspended in a base fluid have been verified to have high thermal conductivity [2]. Recently, through possession of this unique superlative property, they have been the topic of many investigations to enhance the heat transfer rate in various industrial applications.

Although there are some investigations concerning the natural convection phenomenon with nanofluids in enclosures [3], the nanofluid mixed convection flow has received a little attention so far. Tiwari et al. [4], have numerically investigated the behavior of nanofluids inside a two sided lid-driven differentially heated square cavity. They have found that both Richardson number and the direction of moving walls affect the fluid flow and heat transfer in the cavity. Laminar mixed convection flows through a copper-water nanofluid in a square lid driven cavity have been simulated by Talebi et al. [5]. They have studied the effects of solid volume fraction of nanofluids on hydrodynamic and thermal characteristics in a range of the Rayleigh number and the Reynolds number. They have concluded that at the fixed Reynolds number, the solid concentration changes the flow pattern and thermal manner particularly for high Rayleigh numbers. Finally, they have observed that the effect of solid concentration decreases by the increase of Reynolds number. Nemati et al. [6] have applied the lattice Boltzmann method to analyze the mixed convection utilizing a water-based nanofluid containing Cu, Cuo or Al_2O_3 nanoparticles. They have investigated the effects of Reynolds number and solid volume fraction on hydrodaynamic and thermal characteristics. The results obtained by their work indicated that the effect of solid volume fraction became higher for Al_2O_3, Cuo and Cu, in sequential order. Besides, the increase of Reynolds number decreases the solid concentration effect. M. Muthtamilselvan et al. [7] have conducted a numerical study to investigate the transport mechanism of mixed convection in a lid-driven enclosure filled with nanofluids. They have found that both the aspect ratio and solid volume fraction affect the fluid flow and heat transfer in the enclosure. They have also concluded that the variation of the average Nusselt number is linear with solid volume fraction. Effect of wavy wall on convection heat transfer of water-Al_2O_3 nanofluid in a lid-driven cavity is investigated by M. Jafari et al. [8] using Lattice Boltzmann method. M.M. Heyhat and F. Kowsary[9] have used a two-component nonhomogeneous model to simulate forced convection of nanofluids through a circular pipe. Their results have shown that addition of γAl_2O_3 nanoparticles to pure water effectively enhances the convective heat transfer.

The influence of the magnetic field is of great importance in many practical cases such as metal casting, liquid metal cooling for fusion reactors and crystal growth in fluids [10]. Both natural and mixed convection are subjected to forces due to magnetic fields. The steady and laminar natural convection flow in the existence of a magnetic field is examined by Ece and Buyuk [11]. They have found that this field suppressed the convective flow and its direction also influenced the flow pattern. Sivasankaran and Ho [12] numerically investigated the effects of temperature dependent properties on the natural convection of water in a cavity in the presence of a magnetic field. They observed that the heat transfer rate decreases with an increase of the magnetic field and it depends on the direction of the external magnetic field. The unsteady, laminar and mixed convection flow in the presence of internal heat generation or absorption with a magnetic field in an isothermally heated lid driven enclosure is studied by chamkha [1]. He showed that the magnetic field strongly affects flow manner and the heat transfer. Rahman et al. [13]inspected the conjugate effects of joule heating and magneto-hydrodynamics of mixed convection in an obstructed lid driven cavity. They indicated that fluid flow and heat transfer characteristics are highly dependent on the strength of the magnetic field.

Most of the researches on the heat transfer in enclosures with the magnetic field effects are dedicated to examine the electrically conducting fluids with a low thermal conductivity. Recently, Ghasemi et al. [14] studied the natural convection in an enclosure filled with a water-Al_2O_3nanofluid under the influence of a magnetic field. They have indicated that the heat transfer rate decreases with an increase of the Hartmann number. Recently, effects of magnetic field on nanofluid forced convection in a partially heated microchannel are explored by Aminossadati et al. [15]. According to the literature review, to the best knowledge of the authors, no studies have been done before to investigate the problem of mixed convection of a nanofluid in a lid-driven cavity with magnetohydrodynamic effects. Therefore, the effect of

magnetic field on the mixed convection of a nanofluid-filled cavity is investigated here. To do this, an efficient and fully solution-adaptive stencil refinement method [16] is used. This method has superior numerical features compared to fine uniform mesh, such as ability to automatically adjust the local stencil to reflect the transient manner of the solution and thus increase the speed of calculation and greatly save the CPU time. Finally, the influence of several pertinent parameters such as the Reynolds number, the Hartmann number and the solid particle volume fraction on the heat transfer performance of the nanofluid is examined.

2. THE GOVERNING EQUATIONS AND NUMERICAL APPROACH

Figure 1 shows a two-dimensional square cavity of length W and height H that its aspect ratio is taken to be equal to one. The cavity is filled with a suspension of Al_2O_3 nanoparticles in water. As seen from the schematic view, the top wall moves with constant velocity and the two horizontal walls have insulated boundary condition while the temperature at left and right walls is maintained as T_h and T_c, respectively. It is assumed that the nanoparticles are in thermal equilibrium with water. The properties of fluid and nanoparticles are considered to be constant.
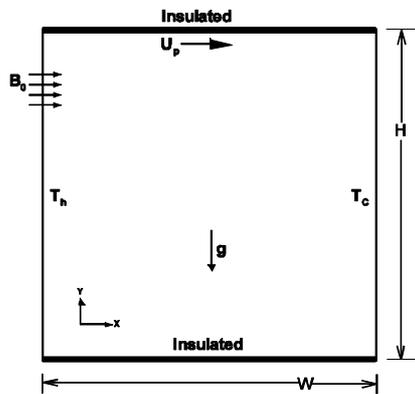

Figure 1. Schematic model of the physical problem

TABLE 1. Thermophysical properties of fluid and nanoparticles at 20 °C [17].

Property	Water	Alumina
c_p(j/kg K)	4179	765
ρ (kg/m^3)	997.1	3970
k (W/mK)	0.613	30
$\beta \times 10^{-5}$ (K^{-1})	21	0.85
d (nm)	0.384	47

The uniform magnetic field B_0 is also applied to the fluid. Table 1 presents thermophysical properties of water and Al_2O_3 nanoparticles [17]. Hence, governing equations can be written in dimensional form as follows:

$$\frac{\partial^2 \psi}{\partial X^2} + \frac{\partial^2 \psi}{\partial Y^2} = -\Omega \tag{1}$$

$$\frac{\partial \Omega}{\partial t} + U\frac{\partial \Omega}{\partial X} + V\frac{\partial \Omega}{\partial Y} = \nu_{nf}(\frac{\partial^2 \Omega}{\partial X^2} + \frac{\partial^2 \Omega}{\partial Y^2}) + \frac{g(\rho\beta)_{nf}}{\rho_{nf}}\frac{\partial(T-T_c)}{\partial X} - \frac{\sigma_{nf}B_0^2}{\rho_{nf}}\frac{\partial V}{\partial X} \tag{2}$$

$$\frac{\partial T}{\partial t} + U\frac{\partial T}{\partial X} + V\frac{\partial T}{\partial Y} = \alpha_{nf}(\frac{\partial^2 T}{\partial X^2} + \frac{\partial^2 T}{\partial Y^2}) \tag{3}$$

where, $U = \frac{\partial \psi}{\partial Y}$, $V = -\frac{\partial \psi}{\partial X}$, and $\alpha_{nf} = k_{nf}/(\rho c_p)_{nf}$.

To define the properties of the nanofluid, the classical models reported in the literature are used [18]

$$\sigma_{nf} = (1-\delta)\sigma_f + \delta\sigma_s \tag{4}$$

$$\rho_{nf} = (1-\delta)\rho_f + \delta\rho_s \tag{5}$$

$$(\rho\beta)_{nf} = (1-\delta)(\rho\beta)_f + \delta(\rho\beta)_s \tag{6}$$

$$(\rho c_p)_{nf} = (1-\delta)(\rho c_p)_f + \delta(\rho c_p)_s \tag{7}$$

The effective viscosity of nanofluid was given by [19] as

$$\mu_{nf} = -0.4491 + \frac{28.837}{T} + 0.574\delta - 0.1634\delta^2 + 23.053(\frac{\delta}{T})^2$$
$$+ 0.0132\delta^3 - 2354.735\frac{\delta}{T^3} + 23.498(\frac{\delta}{d_p})^2 - 3.0185\frac{\delta^3}{d_p^2} \tag{8}$$

The effective thermal conductivity of nanofluid was given by [20]

$$\frac{k_{nf}}{k_f} = 1 + 4.4Re^{0.4}Pr^{0.66}(\frac{T}{T_{fr}})^{10}(\frac{k_p}{k_f})^{0.03}\delta^{0.66} \tag{9}$$

where, Re is the nanoparticle Reynolds number, Pr is the Prandtl number of the base liquid, T is the nanofluid temperature, T_{fr} is the freezing point of the base liquid, k_p is the nanoparticle thermal conductivity, and δ is the volume fraction of the suspended nanoparticles. The nanoparticle Reynolds number is defined as

$$Re_{nf} = \frac{\rho_f u_b d_p}{\mu_f} \tag{10}$$

where, u_b is the Brownian motion velocity of nanoparticle which is defined as:

$$u_b = \frac{2k_b T}{\pi \mu_f d_p^2} \tag{11}$$

Equations (1)–(3) can be converted to the dimensionless forms by definition of the following parameters:

$$X^* = \frac{X}{H}, \; Y^* = \frac{Y}{H}, \; U^* = \frac{U}{U_p}, V^* = \frac{V}{U_p}, \; t^* = \frac{tU_p}{H}, \Omega^* = \frac{\Omega H}{U_p},$$

$$\psi^* = \frac{\psi}{HU_p}, \; T^* = \frac{T - T_c}{T_h - T_c}, \text{Re} = \frac{U_p H}{\nu_f}, \; \text{Pr} = \frac{\nu_f}{\alpha_f}, \tag{12}$$

$$\text{Ra} = \frac{g\beta_f (T_h - T_c)H^3}{\alpha_f \nu_f}, \; \text{Ha} = B_0 H \sqrt{\frac{\sigma_f}{\rho_f \nu_f}}$$

Therefore, using the mentioned parameters leads to dimensionless forms of the governing equations as

$$\frac{\partial^2 \psi^*}{\partial X^{*2}} + \frac{\partial^2 \psi^*}{\partial Y^{*2}} = -\Omega^* \tag{13}$$

$$\frac{\partial \Omega^*}{\partial t^*} + U^* \frac{\partial \Omega^*}{\partial X^*} + V^* \frac{\partial \Omega^*}{\partial Y^*} = \frac{1}{\text{Re}} \frac{\rho_f}{\rho_{nf}} \frac{1}{(1-\delta)^{2.5}} (\frac{\partial^2 \Omega^*}{\partial X^{*2}} + \frac{\partial^2 \Omega^*}{\partial Y^{*2}})$$
$$+ \frac{\text{Ra}}{\text{Pr}\,\text{Re}^2} \frac{(\rho\beta)_{nf}}{\rho_{nf}\beta_f} \frac{\partial T^*}{\partial X^*} - \frac{\sigma_{nf}}{\sigma_f} \frac{\rho_f}{\rho_{nf}} \frac{\text{Ha}^2}{\text{Re}} \frac{\partial V^*}{\partial X^*} \tag{14}$$

$$\frac{\partial T^*}{\partial t^*} + U^* \frac{\partial T^*}{\partial X^*} + V^* \frac{\partial T^*}{\partial Y^*} = \frac{\alpha_{nf}}{\alpha_f} \frac{1}{\text{Re}\,\text{Pr}} (\frac{\partial^2 T^*}{\partial X^{*2}} + \frac{\partial^2 T^*}{\partial Y^{*2}}) \tag{15}$$

The local and average Nusselt number on the left hot wall can be calculated by:

$$\text{Nu}_{Y^*}(Y^*) = -\frac{k_{nf}}{k_f} (\frac{\partial T^*}{\partial X^*})_{X^*=0} \tag{17}$$

$$\text{Nu}_{av} = \int_0^1 \text{Nu}_{Y^*}(Y^*) dY^* \tag{18}$$

The non-dimensional governing equations (Equations (13)-(15)) subject to the boundary conditions (Equation (16)) are solved by the stencil adaptive finite difference method which is proposed by Ding and shu [16]. The 5-points symmetric stencil is guaranteed at each internal node, so that conventional finite difference formula can be easily constructed anywhere in the domain. In general, two types of stencils appear alternatively in this adaptive algorithm which they are shown in Figure 2.

This algorithm is based on the local stencil refining and coarsening using an action indicator which monitors and simultaneously controls the resolution levels of the solution.
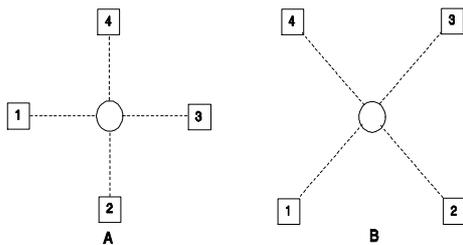

Figure 2. Configuration of the two types of stencils.

In this work, the vorticity and temperature are used as two monitor parameters to measure the local variation of the solution. The space accuracy of the stencil for these computations is second-order and a scheme of fourth-order accuracy is used to interpolate the initial value of dependent variables for the newly inserted nodes. Further details can be found in the ref [16].

To solve the elliptic part of PDEs (Equation (11)), the point Gauss–Seidel iterative method is employed. The solution of the parabolic parts (Equations (12)-(13)), marches in time with a fourth order Runge–Kutta method. The simulation is started on a grid with a 21 × 21 Cartesian mesh as the resolution level 0 and the finest adaptive level is set to 4. Figure 3 show the final node distribution for three different Hartmann numbers (Ha=0, 20, 65) and for a solid particle volume fraction of δ=0.05. The computations are performed until steady-stateconditions are reached. The convergence criterion used in the time loop to achieve steady-state condition is $\left|\varphi^k - \varphi^{k-1}\right| < 10^{-6}$, where φ stands for either T^* or Ω^*.

All the computations are carried out on a personal computer with Pentium Dual-Core Cpu (2G) and Fortran 90 compiler. It can be clearly seen that the node distribution in Figure 3 is quite good in the sense that the stencil resolution levels reflect the local magnitude of the vorticity or temperature variation. It is reasonable to anticipate that these node distributions will be more suitable for the numerical simulation than the uniform node distribution in the sense of efficiency. This expectation is approved by the efficiency comparison presented in Table 2.

As compared with the fixed grid method, this adaptive algorithm needs much less total number of nodes to attain the same accuracy. As a result, the running time is also greatly reduced. It is remarkable that the running time listed in Table 2, embraces the overhead of the stencil adaptation and stencil manipulation.

To validate the present computational code, the results for the MHD natural convection flow in a cavity filled by Al_2O_3-water nanofluid have been compared with those obtained by Ghasemi et al. [14] and Nemati et al. [6, 21]. These comparison revealed good agreements between results which are shown in Figure 4 and Table 3. In addition, Figure 5 depicts another test for validation of this numerical algorithm for the lid-driven square cavity filled by Al_2O_3-water nanofluid. In this test case, vertical velocity on the horizontal centerline has been compared with those of Nemati et al. [6].

3. RESULTS AND DISCUSSION

During the simulations the Prandtl number and the Rayleigh number are fixed at Pr=6.8 and Ra=10^4,

respectively. The effects of the Hartmann number on the streamlines and isotherms are presented in Figures 6a and b, respectively, for three values of Reynolds number (Re=1, 10, 100). The cavity is filled with Al_2O_3-water nanofluid, which has a solid particle volume fraction of $\delta=0.05$. The buoyancy- driven circulating flows are apparent at low Reynolds numbers for all values of Hartmann numbers. The strength of these circulations decreases as the Hartmann number increases. As can be seen from Figure 6a, at Re=100 the flow pattern changes considerably, so that the flow is nearly transformed to the lid-driven cavity flow. Hence, a major mechanically-driven circulating cell is formed. It is observed from the streamlines that this primary cell breaks into two smaller circulating cells when Ha is increased to 65. Figure 6b illustrates that the isotherms are affected by variations in the Hartmann number. They go from horizontal to vertical that would be a sign of weaker convective flows at higher Hartmann numbers.

Figure 7 shows the effects of the Hartmann number on the dimensionless vertical component of velocity (left) and the dimensionless temperature (right) along horizontal centerline at three values of Reynolds number (Re=1, 10, 100) and a solid particle volume fraction of $\delta=0.05$. It is obvious from this figure that for low Reynolds numbers, the effect of buoyancy dominates the forced convection effect. Upward and downward flows are symmetric with respect to the center of the cavity. As can be seen, the increase in the Hartmann number leads to weaken the flow intensity. Thus, due to influence of the magnetic field on the convective flow, the maximum vertical component of velocity decreases when the Hartmann number increases. This influence can also be deduced from temperature curves. The maximum influence of the Hartmann number on the temperature curves is evident at Re=100.

TABLE 2. Efficiency comparison between adaptive algorithm and uniform mesh method ($\delta=0.05$, Ha=65).

	Re	Finest resolution level	Number of nodes	Total iteration number	Running time(s)
Stencil daptive	1	4	3292	29437	537.158
Uniform Mesh	1	81×81	6561	32990	896.974
Stencil daptive	10	4	4279	61423	1515.721
Uniform Mesh	10	81×81	6561	123161	2428.436
Stencil daptive	100	4	4346	35377	780.285
Uniform Mesh	100	81×81	6561	92766	1838.471

TABLE 3. The averaged Nusselt number on the left wall in comparison with the previous study at Ra=10^5.

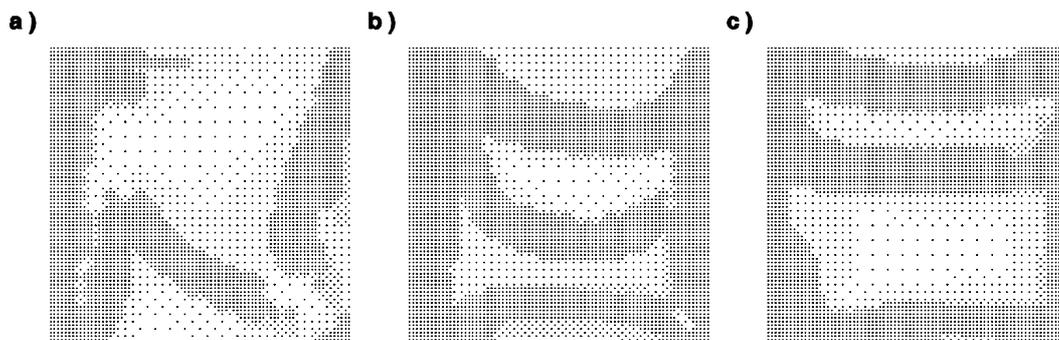|	$\delta=0.00$		$\delta=0.03$		$\delta=0.05$	
Ha	Ref [21]	Present Study	Ref [21]	Present Study	Ref [21]	Present Study
0	3.890	3.901	6.021	6.040	7.499	7.503
10	3.322	3.334	5.313	5.328	6.715	6.723
50	1.303	1.317	1.974	1.980	2.385	2.391
100	1.209	1.222	1.746	1.759	2.178	2.188

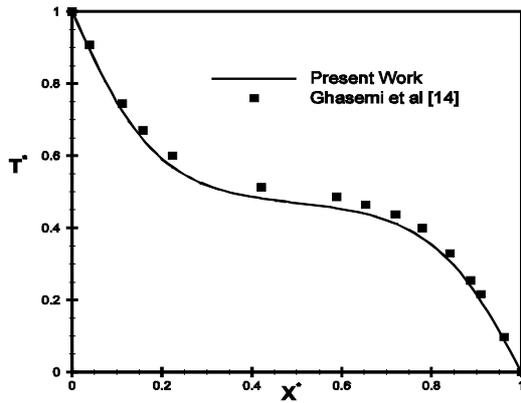**Figure 3.** Final node distribution at Re = 100, $\delta=0.05$: a) Ha=0, b) Ha=20, c) Ha=65

Figure 4. The dimensionless temperature at vertical centerline (δ=0.03, Pr = 6.2, Ra=10^5, Ha=30).
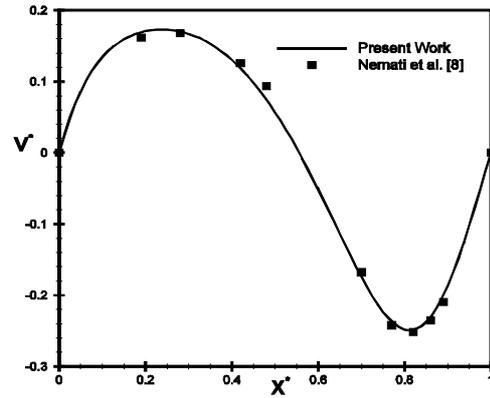

Figure 5. The dimensionless vertical component of velocity on horizontal centerline (δ=0.01, Pr = 6.57, Re=100).
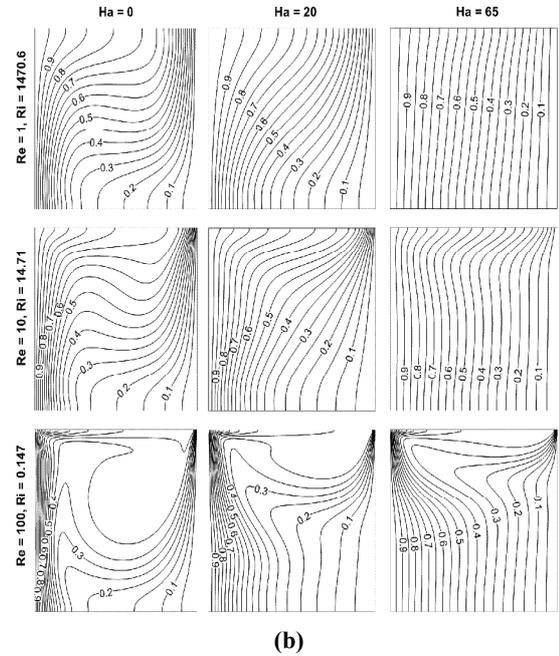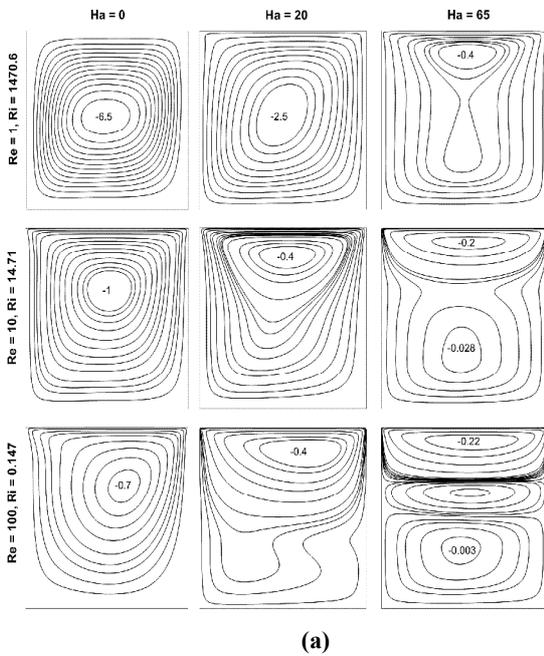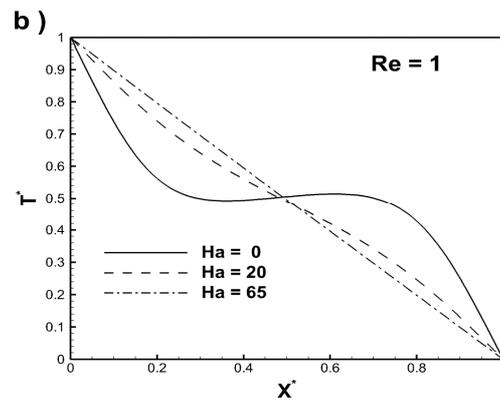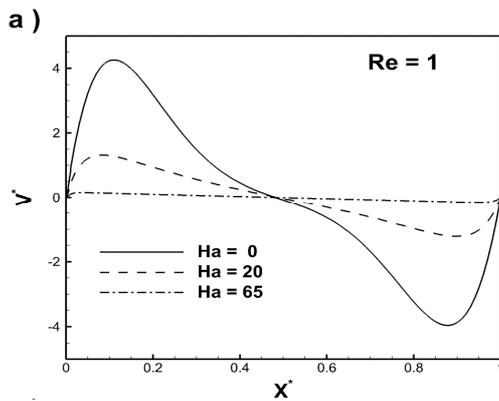

(a)

(b)

Figure 6(a). Streamlines for different Reynolds and Hartmann numbers (δ=0.05), **(b)** Isotherms for different Reynolds and Hartmann numbers (δ=0.05).
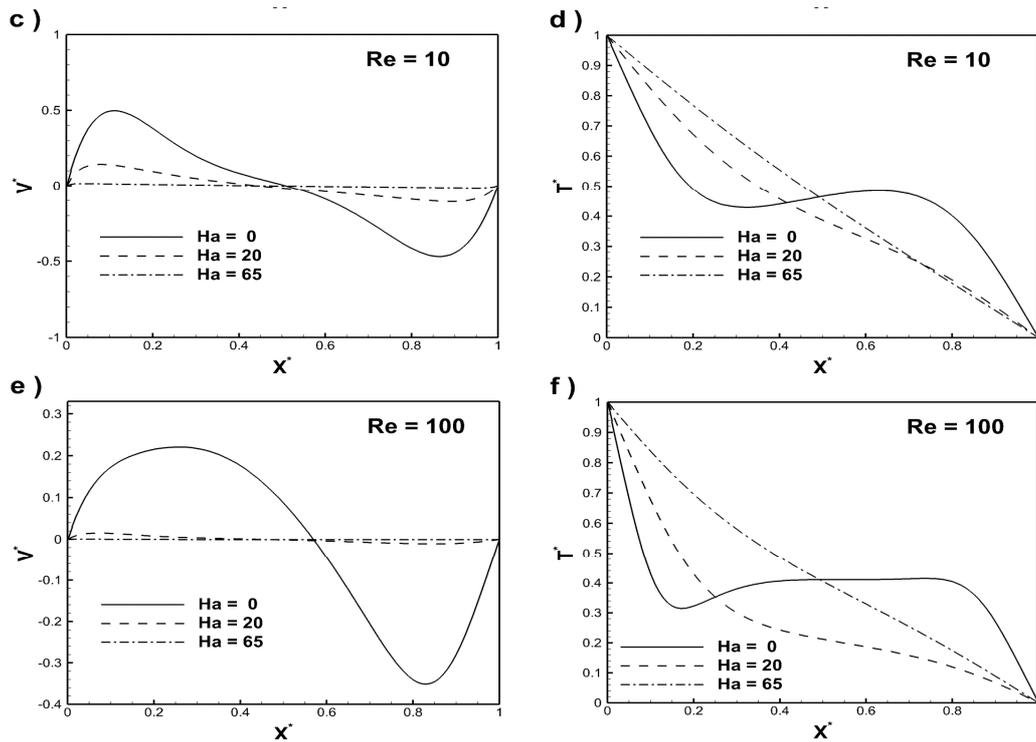
Figure 7. The dimensionless vertical component of velocity (left) and temperature (right) on horizontal centerline (δ=0.05).
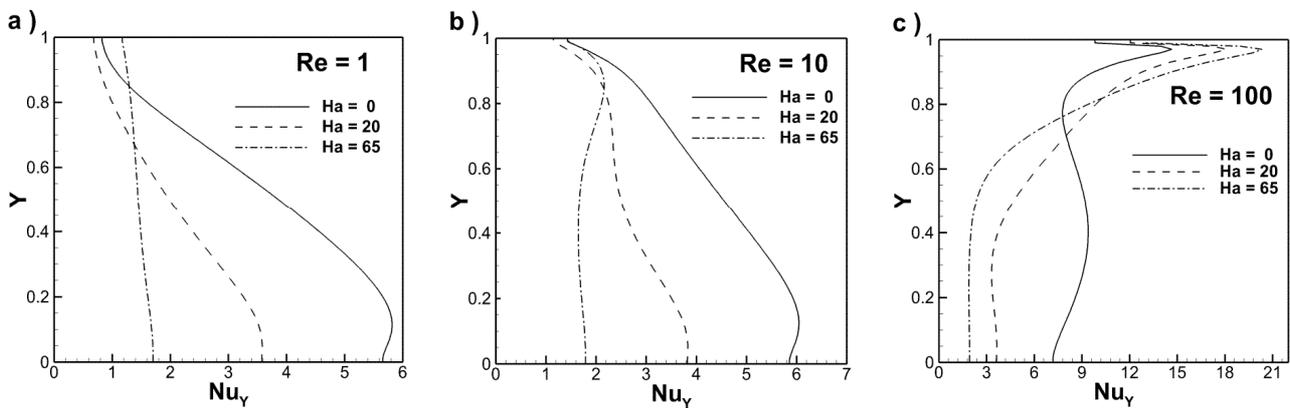

Figure 8. Local Nusselt number at left hot wall (δ=0.05).

The effects of the Hartmann number on the local Nusselt number along the hot wall at three values of Reynolds number (Re=1, 10, 100) is shown in Figure 8. The cavity is filled with Al_2O_3-water nanofluid with a solid particle volume fraction of δ=0.05. The results indicate that the maximum local Nusselt number increase as the Reynolds number increases due to the strengthened convective flow. It decreases as the Hartmann number increases because of suppression of the convective circulating flows at low Reynolds numbers. For Re=100, the maximum local Nusselt number increases when the Hartmann number increases but the average Nusselt number still decreases with an increase in the Hartmann number.

Figure 9 shows the variations of the average Nusselt number with the Hartmann number at different Reynolds numbers when the cavity is filled with a Al_2O_3-water nanofluid (δ=0.05). For all values of the Reynolds number, where the heat transfer is partially or principally convection, the average Nusselt number decreases as the Hartmann number increases because the magnetic fields can suppress the convective flows. This behavior has also been reported by Ghasemi et al. [14] for the case of natural convection.

In order to expose the effects of the magnetic field on the heat transfer, variation of the average Nusselt number ratio $Nu_{av} / Nu_{av,Ha=0}$ has been tracked.
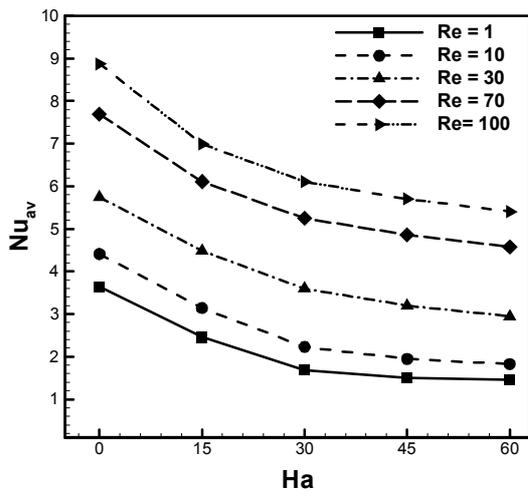
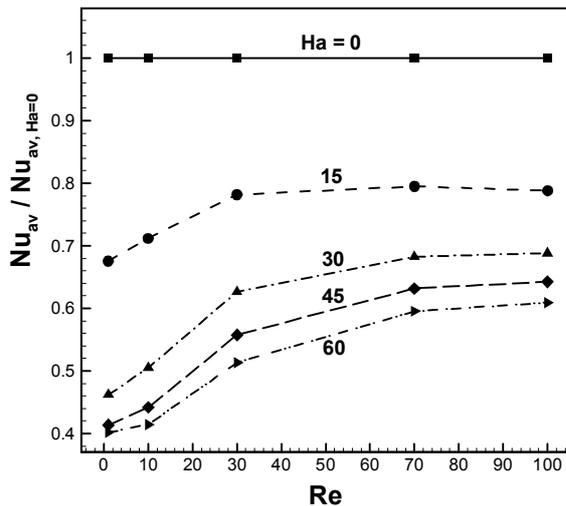**Figure 9.** The average Nusselt number at left hot wall for different Reynolds numbers (δ=0.05).

Figure 10. The average Nusselt number ratio at hot wall for different Hartmann numbers (δ=0.05).

Figure 10 shows how this ratio varies with respect to the Reynolds number at different values of the Hartmann number. For this section of the investigation, the average Nusselt number at Ha=0 is the reference value and the solid particle volume fraction is considered to be constant (δ=0.05). It is clear in Figure 10, that the impact of the Hartmann number on the average Nusselt number ratio decreases as the Reynolds number increases. This can be explained due to the higher convective effects for higher Reynolds numbers. Table 3 demonstrates the effect of the solid particle volume fraction (δ) on the average Nusselt number (Nu_{av}) and the maximum stream function ($| \psi |_{max}$) at different values of the Reynolds number (Re). The Hartmann number is assumed to be Ha=40.

For all values of solid particle volume fraction, the results show that as the Reynolds number increases, Nu_{av} increases but, $| \psi |_{max}$ decreases. An increase of the solid particle volume fraction leads to an increase in the average Nusselt number and the maximum stream function.

At higher Reynolds numbers, an increase of the solid particle volume fraction results in higher values of the average Nusselt number. This is due to the stronger forced convective flows especially at Re=100 that govern the heat transfer process. The fluid manner at this Reynolds number is depicted in Figure 11. This figure illustrates a comparison study between the pure fluid (δ=0) and the nanofluid (δ=0.06) regarding the streamlines and the isotherms at Re=100. The results are provided for three values of the Hartmann number (Ha=0, 40, 75). The results show that the addition of nanoparticles leads to an increase in the maximum stream function in the absence of the magnetic field. However, as the magnetic field is applied, the intensity of convective circulations decreases. That is why the addition of nanoparticles will bring into weaker buoyancy-driven circulations and lower values of the stream function in the existence of magnetic forces.

Variations in the average Nusselt number ratio $Nu_{av} / Nu_{av,\delta=0}$ with the Reynolds number at different values of the solid particle volume fraction are shown in Figure 12. For this section of the investigation, the average Nusselt number at δ=0 is the reference value and the Hartmann number is supposed to be constant (Ha=40). The results demonstrate that for the nanofluid, which is influenced by a magnetic field (Ha=40), the average Nusselt number ratio increases with an increase in the solid particle volume fraction in whole range of Reynolds numbers. The important point in Figure 12 is that there is a critical Reynolds number ($Re_{crit} \cong 30$) where the addition of the solid particles has its minimum effect on the heat transfer enhancement, regardless of the value of the solid particle volume fraction.

To provide a better understanding of the heat transfer behavior of the cavity at Re=100, the variations of Nu_{av} and $|\psi|_{max}$ with the solid particle volume fraction at different Hartmann numbers is inspected in Table 4. The results show that the Hartmann number has an important role in the efficiency of the solid particles in enhancement of the heat transfer performance. As the Hartmann number increases, the heat transfer rate (Nu_{av}) decreases; but, the addition of the solid particles to the base fluid enhances the heat transfer performance.

Figure 13 shows the variation in the average Nusselt number ratio ($Nu_{av} / Nu_{av,\delta=0}$) with the Hartmann number at different solid particle volume fractions. The results, which are presented for Re=100,

show that as the Hartmann number increases, the rate of increase in the average Nusselt number ratio due to addition of the solid particles decreases as a result of stronger magnetic flows.
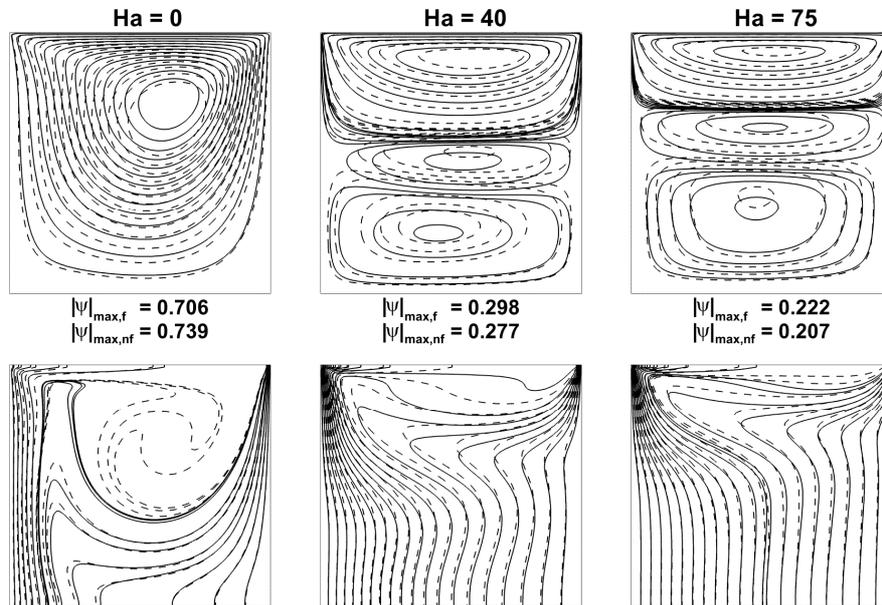

Figure 11. Streamlines (left) and isotherms (right) at Re=100, Pure fluid (—) and nanofluid with δ=0.06 (- - -).

TABLE 3. Average Nusselt number at various Re and δ (Ha=40).

		Re=1	Re=10	Re=30	Re=70	Re=100
δ=0 .00	$|\psi|_{max}$	0.749	0.319	0.301	0.299	0.298
	Nu_{av}	1.107	1.590	2.665	3.917	4.590
δ=0 .02	$|\psi|_{max}$	0.758	0.289	0.273	0.272	0.272
	Nu_{av}	1.348	1.784	2.951	4.423	5.182
δ=0 .04	$|\psi|_{max}$	0.762	0.292	0.276	0.274	0.274
	Nu_{av}	1.482	1.944	3.202	4.808	5.631
δ=0 .06	$|\psi|_{max}$	0.765	0.295	0.279	0.277	0.277
	Nu_{av}	1.594	2.076	3.408	5.122	5.996

TABLE 4. Average Nusselt number at various Ha and δ (Re=100).

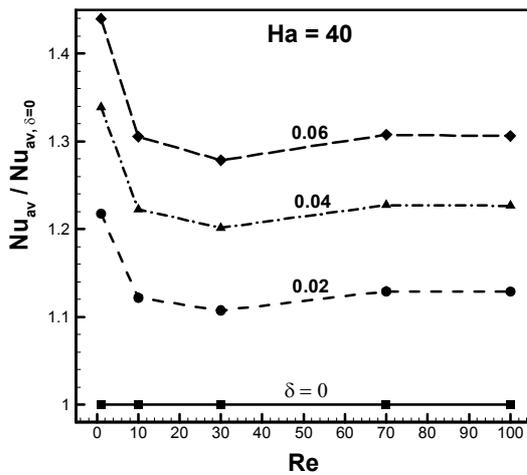|		Ha = 0	Ha =15	Ha = 30	Ha = 45	Ha = 60	Ha = 75
δ=0 .00	$|\psi|_{max}$	0.706	0.457	0.0506	0.0420	0.0366	0.0328
	Nu_{av}	6.489	5.458	5.874	5.104	4.634	4.291
δ=0 .02	$|\psi|_{max}$	0.736	0.423	0.0505	0.0419	0.0365	0.0328
	Nu_{av}	7.900	6.224	5.967	5.185	4.723	4.406
δ=0 .04	$|\psi|_{max}$	0.738	0.427	0.0504	0.0418	0.0365	0.0327
	Nu_{av}	8.586	6.765	6.057	5.272	4.817	4.508
δ=0 .06	$|\psi|_{max}$	0.739	0.431	0.0504	0.0418	0.0365	0.0327
	Nu_{av}	9.139	7.203	6.150	5.365	4.998	4.616

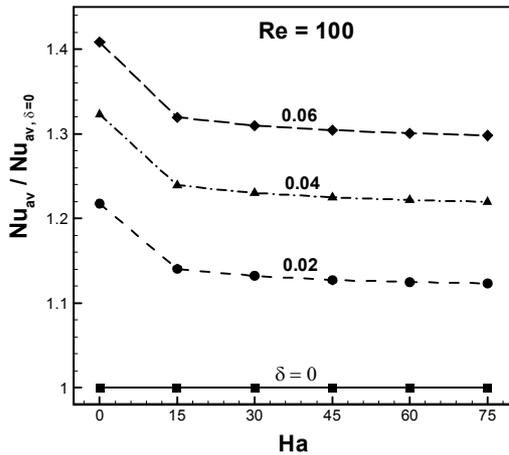**Figure 12.** Variation of average Nusselt number ratio with Reynolds number (Ha=40).

Figure 13. The average Nusselt number ratio at hot wall for different Hartmann numbers (δ=0.05).

4. CONCLUSION

MHD mixed convection in a lid-driven cavity filled with nanofluid is studied numerically using an adaptive stencil finite difference method. Results for various parametric conditions are presented and discussed. Based on the obtained results, it can be concluded that the stencil adaptive method could be and should be considered as a perfect numerical approach. Furthermore, the following conclusions can be drawn from this study:

- The Reynolds number and the Hartmann number play important roles in changing the heat transfer mechanism which dominates the flow field. As the Reynolds number increases, the consequent enhanced convective properties cause a higher heat transfer rate but a higher Hartmann number results in weaker

convective flows and hence lower heat transfer rates.
- The curves of the local Nusselt number along the hot wall and the average Nusselt number ratio confirm that when the Hartmann number increases, the heat transfer rate decreases. The rate of this decrease is dependent on the Reynolds number.
- For a fixed magnetic field, the heat transfer rate increases as Reynolds number increases due to enhanced convective flows.
- For a fixed magnetic field, the heat transfer rate increases as Reynolds number increases due to enhanced convective flows.
- The effect of the solid particle volume fraction on the heat transfer rate highly depends on the values of the Reynolds number and the Hartmann number. For Ha=40, the curves of average Nusselt number ratio with respect to Reynolds number has a minimum point where the nanofluid has its minimum effect on the heat transfer performance.

5. REFERENCES

1. Chamkha, A. J., "Hydromagnetic combined convection flow in a vertical lid-driven cavity with internal heat generation or absorption", *Numerical Heat Transfer: Part A: Applications*, Vol. 41, No. 5, (2002), 529-546.

2. Choi, S. U. and Eastman, J., Enhancing thermal conductivity of fluids with nanoparticles., Argonne National Lab., IL United States.(1995)

3. Jou, R.-Y. and Tzeng, S.-C., "Numerical research of nature convective heat transfer enhancement filled with nanofluids in rectangular enclosures ,"*International Communications in Heat and Mass Transfer*, Vol. 33, No. 6, (2006), 727-736.

4. Tiwari, R. K. and Das, M. K., "Heat transfer augmentation in a two-sided lid-driven differentially heated square cavity utilizing nanofluids", *International Journal of Heat and Mass Transfer*, Vol. 50, No. 9, (2007), 2002-2018.

5. Talebi, F., Mahmoudi, A. H. and Shahi, M., "Numerical study of mixed convection flows in a square lid-driven cavity utilizing nanofluid", *International Communications in Heat and Mass Transfer*, Vol. 37, No. 1, (2010), 79-90.

6. Nemati, H., Farhadi, M., Sedighi, K., Fattahi, E. and Darzi, A., "Lattice boltzmann simulation of nanofluid in lid-driven cavity", *International Communications in Heat and Mass Transfer*, Vol. 37, No. 10, (2010), 1534-1528

7. Muthtamilselvan, M., Kandaswamy, P. and Lee, J., "Heat transfer enhancement of copper-water nanofluids in a lid-driven enclosure", *Communications in Nonlinear Science and Numerical Simulation*, Vol. 15, No. 6, (2010), 1501-1510.

8. afari ,M., Farhadi, M., Sedighi, K. and Fattahi, E., "Effect of wavy wall on convection heat transfer of water-al2o3 nanofluid in a lid-driven cavity using lattice boltzmann method", *International Journal of Engineering-Transactions A: Basics*, Vol. 25, No. 2 (2012)1560-1568

9. Heyhat, M. and Kowsary, F., "Numerical simulation of forced convection of nanofluids by a two-component nonhomogenious model", *International Journal of Engineering, Transactions A: Basics*, Vol. 23, No. 1, (2010), 89-99.

10. M., M., "Magnetohydrodynamics", The Netherlands, (1990).

11. Ece, M. C. and Büyük, E., "Natural-convection flow under a magnetic field in an inclined rectangular enclosure heated and

cooled on adjacent walls", *Fluid Dynamics Research*, Vol. 38, No. 8, (2006), 564-590.

12. Sivasankaran, S. and Ho, C.-J., "Effect of temperature dependent properties on mhd convection of water near its density maximum in a square cavity", *International Journal of Thermal Sciences*, Vol. 47, No. 9, (2008), 1184-1194.

13. Rahman, M., Alim, M .and Sarker, M., "Numerical study on the conjugate effect of joule heating and magnato-hydrodynamics mixed convection in an obstructed lid-driven square cavity", *International Communications in Heat and Mass Transfer*, Vol. 37, No. 5, (2010), 524-534.

14. Ghasemi, B., Aminossadati, S. and Raisi, A., "Magnetic field effect on natural convection in a nanofluid-filled square enclosure", *International Journal of Thermal Sciences*, Vol. 50, No. 9, (2011), 1748-1756.

15. Aminossadati, S., Raisi, A. and Ghasemi ,B., "Effects of magnetic field on nanofluid forced convection in a partially heated microchannel", *International Journal of Non-Linear Mechanics*, Vol. 46, No. 10, (2011), 1373-1382.

16. Ding, H. and Shu, C., "A stencil adaptive algorithm for finite difference solution of incompressible viscous flows", *Journal of Computational Physics*, Vol. 214, No. 1, (2006), 397-420.

17. "Http://www.Matweb.Com/, in.",

18. Xuan, Y. and Roetzel, W., "Conceptions for heat transfer correlation of nanofluids ,"*International Journal of Heat and Mass Transfer*, Vol. 43, No. 19, (2000), 3701-3707.

19. Khanafer, K. and Vafai, K., "A critical synthesis of thermophysical characteristics of nanofluids", *International Journal of Heat and Mass Transfer*, Vol. 54, No. 19, (2011), 4428-44100,

20. Corcione, M., "Empirical correlating equations for predicting the effective thermal conductivity and dynamic viscosity of nanofluids", *Energy Conversion and Management*, Vol. 52, No. 1, (2011), 789-793.

21. Nemati, H., Farhadi, M ,.Sedighi, K., Ashorynejad, H. and Fattahi, E., "Magnetic field effects on natural convection flow of nanofluid in a rectangular cavity using the lattice boltzmann model", *Scientia Iranica*, Vol. 19, No. 2, (2012), 303-310.

Numerical Investigation of Magnetic Field Effects on Mixed Convection Flow in a Nanofluid-filled Lid-driven Cavity

J. Rahmannezhad[a], A. Ramezani[b], M. Kalteh[c]

[a] Department of Mechanical Engineering, University of Birjand, Birjand, Iran
[b] Faculty of Aerospace Engineering, K.N. Toosi University of Technology, Tehran, Iran
[c] Department of Mechanical Engineering, University of Guilan, Rasht, Iran

چکیده

در این کار، الگوریتم الگوی تطبیقی برای مطالعه اثرات میدان مغناطیسی بر روی انتقال حرارت ترکیبی نانو سیال آب–
اکسید آلومینیوم درون یک حفره مربعی، به کار گرفته شده است. معادلات تراکم ناپذیرناویر–استوکس با به کار گیری یک
روش تطبیقی تولید شبکه که برتریهای خوبی نسبت به روشهای سنتی بر روی شبکههای یکنواخت ریز دارد، حل شدهاند.
هدف اصلی این تحقیق بررسی اثر چندین پارامتر مهم مانند عدد رینولدز، عدد هارتمن و کسر حجمی ذرات جامد بر روی
نحوه انتقال حرارت نانوسیال است. بر اساس نتایج عددی حاصله، نرخ انتقال حرارت با افزایش عدد رینولدز افزایش می-
یابد اما با افزایش عدد هارتمن این نرخ کاهش مییابد. همچنین، نتایج نشان میدهند که میزان بهبود عملکرد انتقال حرارت
نانوسیال نسبت به سیال پایه به عدد رینولدز جریان وابسته است.

doi: *10.5829/idosi.ije.2013.26.10a.11*